JOURNAL OF SYNCHROTRON RADIATION

ISSN 1600-5775

In situ beamline analysis and correction of active optics. Erratum

John Sutter,* Simon Alcock and Kawal Sawhney

Diamond Light Source Ltd, Harwell Science and Innovation Campus, Chilton, Didcot, Oxfordshire OX11 0DE, UK. *Correspondence e-mail: john.sutter@diamond.ac.uk

Received 17 July 2017
Accepted 17 July 2017

Keywords: *in situ*; correction; X-ray; mirror.

A correction to one of the equations in the paper by Sutter *et al.* (2012). [*J. Synchrotron Rad.* **19**, 960–968] is made.

Equation (5) in the paper by Sutter *et al.* (2012) should be

$$B(x) = \frac{(C_1 + C_2)\,x}{2EI} + \frac{(C_1 - C_2)\,x^2}{2LEI}. \qquad (5)$$

Note the additional factor of 2 in the denominator of the quadratic term on the right-hand side.

References

Sutter, J., Alcock, S. & Sawhney, K. (2012). *J. Synchrotron Rad.* **19**, 960–968.

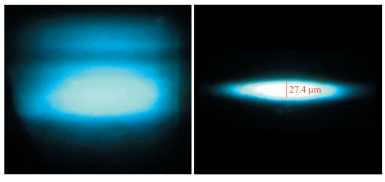

Journal of
Synchrotron Radiation

ISSN 0909-0495

Received 14 April 2012
Accepted 22 August 2012

In situ beamline analysis and correction of active optics

John Sutter,* Simon Alcock and Kawal Sawhney

Diamond Light Source Ltd, Harwell Science and Innovation Campus, Chilton, Didcot, Oxfordshire OX11 0DE, UK. E-mail: john.sutter@diamond.ac.uk

At the Diamond Light Source, pencil-beam measurements have enabled long-wavelength slope errors on X-ray mirror surfaces to be examined under ultra-high vacuum and beamline mounting without the need to remove the mirror from the beamline. For an active mirror an automated procedure has been implemented to calculate the actuator settings that optimize its figure. More recently, this *in situ* pencil-beam method has been applied to additional uses for which *ex situ* measurements would be inconvenient or simply impossible. First, it has been used to check the stability of the slope errors of several bimorph mirrors at intervals of several weeks or months. Then, it also proved useful for the adjustment of bender and sag compensation actuators on mechanically bent mirrors. Fits to the bending of ideal beams have been performed on the slope errors of a mechanically bent mirror in order to distinguish curvatures introduced by the bending actuators from gravitational distortion. Application of the optimization procedure to another mechanically bent mirror led to an improvement of its sag compensation mechanism.

Keywords: *in situ*; correction; X-ray; mirror.

1. Introduction

The pencil-beam scanning technique is used at many synchrotron light sources to optimize active focusing mirror systems. Series of pencil-beam scans with sequentially incremented actuator settings are used to calculate the adjustments necessary for focusing. This has been done by Hignette *et al.* (1997) and by others since. Now this method has been implemented at Diamond Light Source. The authors' previous report (Sutter *et al.*, 2011) shows in detail how the scanning procedure was automated to save time and effort while maintaining an accuracy similar to that of *ex situ* profilometry. Except for a simple visible-light camera with scintillator, only equipment already installed at the beamlines was used. Moreover, all code for running scans and calculating the actuator corrections was written in the widely available Jython language. Tests performed at several beamlines at Diamond Light Source showed that Diamond's implementation effectively improved the focal quality and also permitted the deliberate controlled defocusing of a beam at a sample. The pencil-beam scans were shown to be both reproducible and in good agreement with *ex situ* measurements carried out in-house. Thus, Diamond's application of this method has met, in a simple and cost-effective way, the requirements fulfilled earlier by the *in situ* long-trace profiler (Qian *et al.*, 1995): accuracy, repeatability, insensitivity to the environment and of course versatility. It has done so without the need to break the ultra-high vacuum in which the optics must normally operate.

As Diamond's implementation of the *in situ* pencil-beam method has developed, new applications have been found for it. The present report provides examples of (i) examinations of the stability of the surface figures of bimorph mirrors over periods up to two years, (ii) discovery of faults on a mirror's surface and of practical ways to remove them, (iii) diagnosis of actuators that are out of range or malfunctioning, (iv) calculation of actuator settings for a collimating mirror.

At Diamond Light Source, *in situ* pencil-beam measurements and *ex situ* profilometric measurements are used together to help beamlines obtain the best possible performance from their active optics. The *in situ* and *ex situ* measurements led to the same conclusions wherever both were possible. For example, a corrugation on the bimorph mirror surfaces that could not be corrected using the electrodes was discovered by both methods and was corrected by repolishing. Large and bulky mirror systems, however, sometimes cannot be inspected *ex situ* at all. This was true for the mechanically bent vertical focusing mirror (VFM) of Diamond's Extreme Conditions beamline I15 and for the collimating mirror at Diamond's X-ray absorption spectroscopy beamline I20. Both of these mirrors have an actuator to correct their gravitational distortion, but this actuator is embedded in a bulky frame of preloaded springs that is too large to be placed on a long-trace profiler or any similar instrument. Therefore, the setting of the gravitational sag compensation can be optimized only with *in situ* measurements. The case of I15 was especially dramatic because its initial poor focusing performance was in fact

caused by incorrect preloading of the sag compensation actuator. Once this was corrected, the focusing improved greatly. Similarly, although the forces applied by the actuators of a mechanically bent mirror are often calibrated by the manufacturer using finite-element analysis, *in situ* measurements are the only sure way of knowing whether the manufacturer's simulations are accurate. This proved especially true for the collimating mirror at beamline I20, for which a fitting function based on a simple model of elastic bending will here be applied to pencil-beam scans to obtain the optimal setting of its sag compensation mechanism.

2. Instrumentation

The pencil-beam method has been implemented for grazing-incidence (2–3 mrad) mirrors at Diamond Light Source as shown in Fig. 1. A scannable slit that is permanently installed upstream from the mirror is closed to a very small size so that only several millimeters of the mirror are illuminated at any one time. The slit widths were generally not well calibrated, but were chosen empirically by examining the image of the reflected beam in the camera. The slit was closed until no image could be recorded, then opened by about 10–20 µm. At the photon energies used in these measurements (12–18 keV up to 50 keV) this was wide enough to prevent broadening by diffraction. In each pencil-beam scan, no less than two to three slit positions were taken per actuator in order to include all spatial frequencies up to the highest that the actuators could correct. In fine pencil-beam scans for detailed measurements of the bimorph mirrors' surface slope error, up to eight slit positions per electrode were recorded. A variation δy in reflected beam position can be converted to a variation δs in mirror slope by the simple formula

$$\delta s = \delta y/2D, \tag{1}$$

where D is the distance from the mirror to the camera.

Knowledge of the influence of each actuator on the entire optic is required in order to calculate the optimal actuator settings for a given purpose. This can be gained by acquiring a series of $n + 1$ scans over m slit positions, where n is the number of actuators that control the optic. The first scan is taken with some arbitrary set of actuator settings. Then the first actuator setting is incremented by some amount v and a second scan is taken. The second actuator setting is likewise incremented by v before the third scan, and so forth until all n actuator settings have been incremented. Subtracting the jth scan from the $(j + 1)$th scan yields the response of the jth actuator. An $m \times n$ interaction matrix H, whose columns are the responses of the actuators per unit change in setting, is defined as

$$H_{ij} = \left(y_{i,j+1} - y_{ij}\right)/v, \tag{2}$$

where y_{ij} is the centroid position of the beam reflected from the ith section of the mirror in the jth scan. Now define an $m \times 1$ vector Y, where Y_i is the correction needed to shift the beam reflected from the ith section of the mirror in the initial scan to its desired position. Also define a $n \times 1$ vector V, where V_j is the correction to the setting on the jth actuator. The shortest-length least-squares solution for V is $H^{\dagger}Y$, where $H^{\dagger}$ is the $n \times m$ Moore–Penrose pseudoinverse of H. The pseudoinverse is unique and can be calculated by singular value decomposition using common numerical linear algebra routines as discussed below.

For *in situ* measurements of mirror slope error on beamlines that did not have their own beam imaging systems, an X-ray camera was built in-house. This device, displayed in Fig. 2, was designed and assembled from off-the-shelf components according to a previous design (Koch *et al.*, 1998; Martin & Koch, 2006). A single-crystal Ce-doped YAG scintillator generates visible light when exposed to X-rays. This light is reflected by a mirror so that the lens and CCD camera are kept out of the X-rays. The lens creates an image of the scintillator on the CCD camera. The spatial resolution of this imaging system depends on the pixel size of the CCD, the

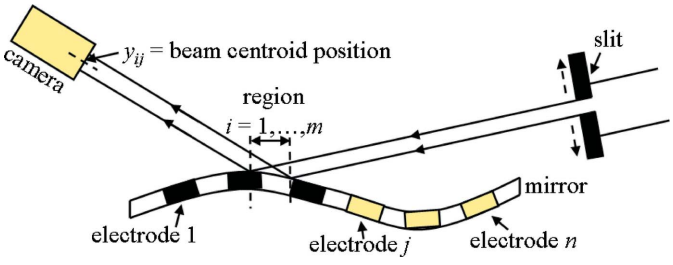

Figure 1
Schematic of the jth scan of the *in situ* pencil-beam procedure as implemented at Diamond Light Source for bimorph mirrors. A small slit upstream from the mirror illuminates the ith section of the mirror's surface. A total of m slit positions are scanned. Of the bimorph mirror's n electrodes, electrodes 1 to $j - 1$ have been incremented. The centroid y_{ij} of the beam reflected from the ith section of the mirror during the jth scan is calculated from the image recorded by the camera. For mechanical mirrors the principle is the same, except that instead of electrodes there are mechanical actuators.

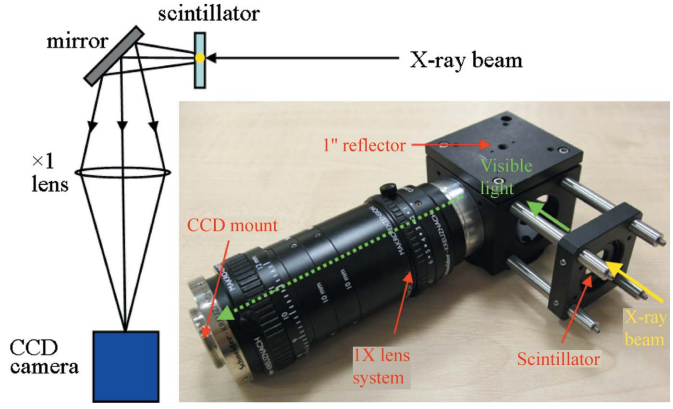

Figure 2
Schematic and photograph of the X-ray camera used for *in situ* measurements at Diamond Light Source. The scintillator is a 100 µm-thick Ce-doped YAG single crystal. The lens has a magnification of 1, a focal length of 50 mm and an f-number of 2.8. The original CCD camera contained 1032 × 776 pixels, each of size 4.65 µm × 4.65 µm, but the C mount allowed other CCD cameras to be used when needed. This camera was used at beamlines that did not have their own sample imaging systems.

thickness z of the scintillator and the numerical aperture N of the lens. For optimal results the lens's depth of focus should match the scintillator's thickness. In calculating the 90% integrated line spread function, the contribution R_{SL} of the scintillator and the lens to the total spatial resolution is given by

$$R_{SL} = \left[(p/N)^2 + (qzN)^2\right]^{1/2}, \quad (3)$$

where $p = 0.70$ µm and $q = 0.28$. R_{SL} and z are in micrometers. For the 100 µm-thick scintillator used here, R_{SL} = 6.35 µm, which is larger than the pixel size of the CCD (maximum 4.65 µm per pixel). Images of the focused undulator beams were captured with exposures of a few tenths of a second.

The beamline motors and X-ray camera image collection were user-controlled through EPICS (EPICS, 2010). The pencil-beam scans were executed and processed through the Generic Data Acquisition (GDA) framework, a Java/Eclipse-based distributed system with an embedded Jython scripting environment, open-sourced since late 2009 (OpenGDA, 2010). Two Jython scripts were composed, one for calculating the centroid position of a beam image by performing a two-dimensional Gaussian fit, the other for calculating and inverting the interaction matrix. Note that the calculation of the centroid was found to be reproducible to within about 0.1 pixel (Sutter *et al.*, 2011) and therefore was not constrained by the much larger value of R_{SL}. Thus the entire procedure for optimizing the actuators is automated.

All *ex situ* measurements reported here were made on the Diamond-NOM (Alcock *et al.*, 2010), a slope-measuring profiler.

3. Results

3.1. Bimorph inspections

In situ measurements of the slope error profile of the bimorph mirrors installed at several beamlines at Diamond Light Source revealed a strong periodic structure or corrugation that was subsequently confirmed by *ex situ* measurements taken on the Diamond-NOM. *Ex situ* inspection (Fig. 3) showed that the jumps in slope error are located at the junctions where the piezoelectric plates are bonded together. Similar corrugations have been reported previously (Sutter *et al.*, 2011). A new example, the VFM of beamline I22, which shows the best agreement between *ex situ* and *in situ* measurements achieved so far, is shown in Fig. 4. In all these examples the corrugation raised the r.m.s. slope error as high as 3.9 µrad. This was considerably above the original slope error specification of 2.0 µrad given to the manufacturer. Because this structure appears on so many bimorph mirrors and degrades the focusing performance significantly, much attention has been paid to it. At the same time it has provided an opportunity to show that the pencil-beam method yields consistent measurements of slope error over long periods of time.

Fig. 5 shows *in situ* pencil-beam measurements made on the rhodium stripe of a vertically focusing mirror before and after

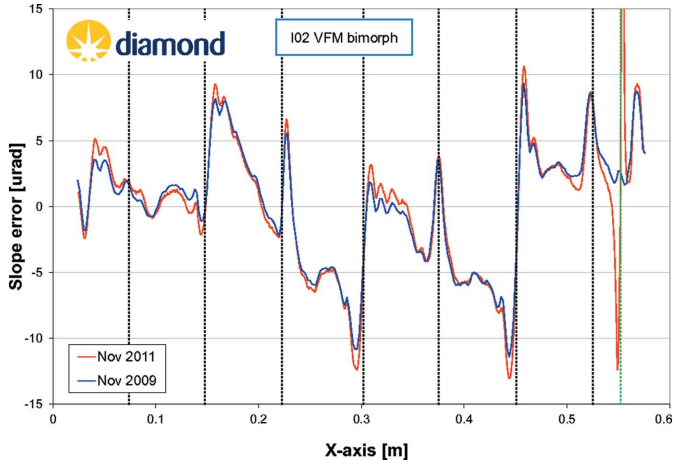

Figure 3
Two *ex situ* slope error scans of the I02 VFM taken two years apart. The vertical dotted lines indicate the junctions of the piezoelectric plates. Note that the only observed change in the surface features is the appearance of a spike at the far right-hand edge of the mirror (about 0.55 m). Visual inspection showed that the spike coincided with a burn mark.

repolishing. Note that the r.m.s. slope error has been reduced from almost 4 µrad to about 0.42 µrad. The four sets of *in situ* data taken over the three-month period after the mirror's re-installation agree very well, and show no sign that the surface is deteriorating. Such frequent inspection of a mirror over such an extended period could not have been done *ex situ* without severe loss of operating time to the beamline, but each *in situ* inspection required only a few minutes of beam time. The images in Fig. 6 confirm that the vertical profile was enormously improved by the repolishing. The beam before repolishing was too wide to measure with a wire scan, but afterwards a series of wire scans confirmed that the vertical profile is now smooth and narrow, with a FWHM size of about 18.5 µm. The theoretical vertical width of the beam may be estimated from the r.m.s. electron beam size (4.2 µm) and the r.m.s. slope error of 0.42 µrad times twice the mirror–sample

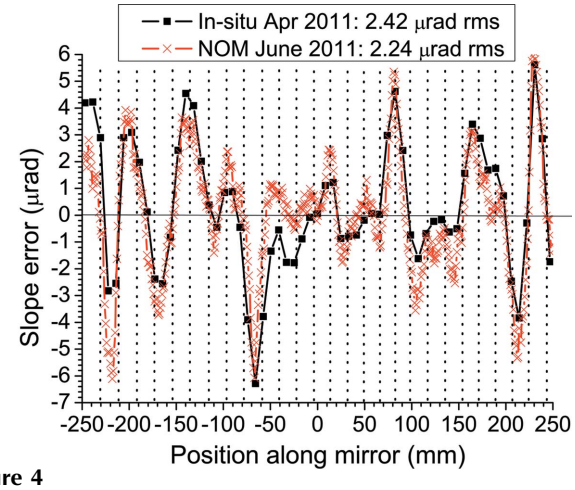

Figure 4
In situ pencil-beam scans collected from the active area of the I22 VFM compared with *ex situ* scans made with the Diamond-NOM. The vertical dotted lines show the locations of the junctions between the electrodes.

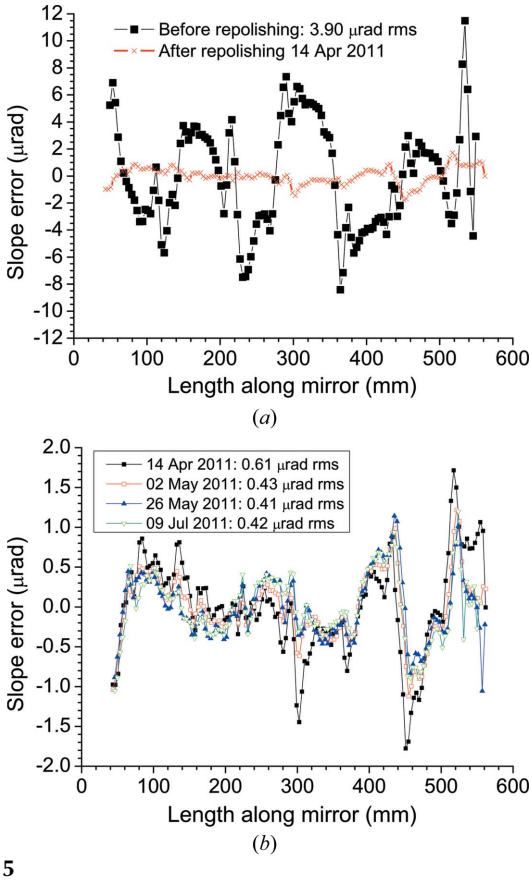

Figure 5
(*a*) Slope error of a rhodium stripe of VFM measured *in situ* before repolishing (in I04) and after repolishing (in I03). Note the great improvement to the mirror's surface. (*b*) Slope errors after repolishing shown on enlarged vertical scale for clarity. Note the stability of the slope errors over time.

distance of 6.885 m (5.78 μm). The sum of these in quadrature yields an r.m.s. vertical width of 7.15 μm or a FWHM of 16.8 μm for the focused beam, which agrees well with the measurement.

Other bimorph mirrors that were not repolished were nonetheless re-examined to check their stability. Fig. 7 shows a series of three scans taken on the I19 horizontally focusing mirror (HFM), two on the rhodium stripe and one on the platinum stripe. Note the similarity not only between the two scans on the Rh stripe taken over a year apart but also between the Rh stripe and the Pt stripe. This indicates that the corrugation of the bimorph mirror extends across its whole width and is not caused by imperfections in the coating procedure. In all these cases deterioration of the surface quality during routine operation has been found not to occur.

3.2. Mechanically bent mirror inspections and analysis

3.2.1. Theory and application to collimating mirror at beamline I20. The utility of *in situ* pencil-beam scans is not restricted to bimorph mirrors. Inspections of the VFM on Diamond's Extreme Conditions beamline I15 and of the vertical collimating mirror on the X-ray Spectroscopy beamline I20 prove this point. Each of these mirrors has a rectangular profile with independently actuated bending moments applied to each end to curve the mirror to an approximately elliptical or parabolic shape. To compensate for the distortion caused by gravity, each mirror has a double support connected to a motor through a set of preloaded springs. The rotation of the motor sets the upward force that the support applies to the mirror.

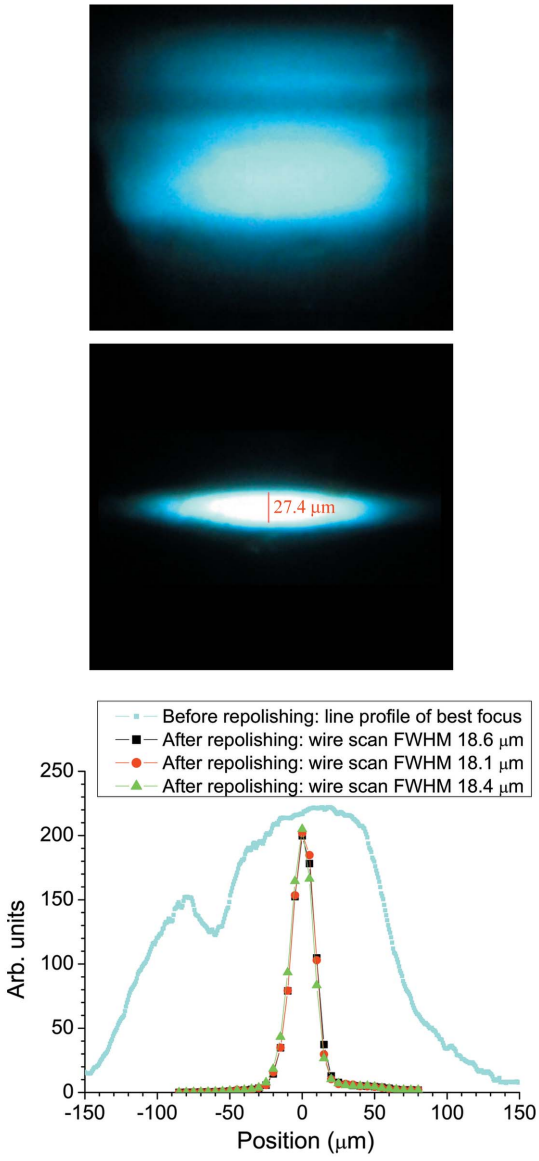

Figure 6
(Top) Image from the inline viewing system of the best achieved focal profile of the beam reflected by the I04 VFM before repolishing. (Center) Image of the best achieved focal profile of the beam reflected by the same mirror at I03 after repolishing. Both images are on the same scale, which is shown by the mark at the center of the second image. (Bottom) Vertical line profile of the best focus before repolishing, compared with three consecutive wire scans of the vertical profile of the focused beam after repolishing.

Although finite-element analysis is often most appropriate for simulating the deformation of a mirror under realistic mechanical and thermal loads, for simplicity mirrors are often treated as though they were elastically bent beams. In this discussion a beam is defined as a piece of material whose

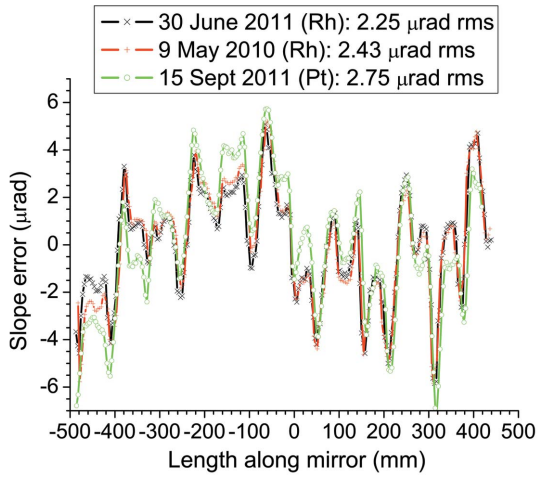

Figure 7
In situ pencil-beam scans collected from the I19 HFM on both its rhodium (Rh) and its platinum (Pt) reflective stripes. Collection dates are shown in the figure. Note here also the absence of significant change in the mirror figure over time.

length is much greater than its width or thickness. The beam is assumed to have at least one longitudinal plane of symmetry, and all the loads and reactions are assumed to lie in such a plane. The forces applied to the beam are also assumed to be perpendicular to the beam's length. Following the treatment of Howells & Lunt (1993), let x be the coordinate along the beam's length (with the center at $x = 0$ and positive x toward the X-ray source) and let y be the deformation at right angles to the beam's length. Then, if the deformation owing to shear is neglected, the shape of the beam can be solved from the differential equation given by Roark & Young (1975). [Calculations of a bending beam that include shear are covered by Timoshenko's theory (Timoshenko, 1921, 1922), which has not been applied here.]

Standard vertical focusing mirrors are generally flat slabs that are mounted on two symmetrically located support points, with additional 'prop load' forces applied at two symmetrically located points between the supports (Fig. 8). The prop loads

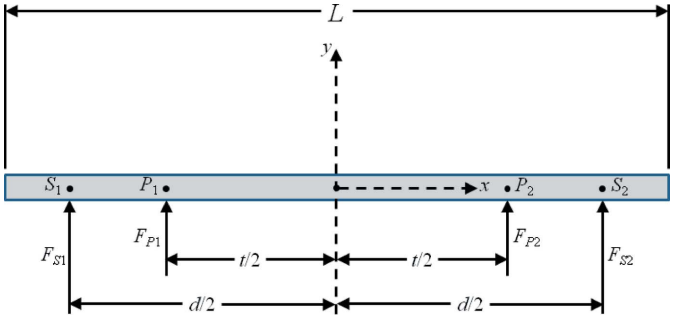

Figure 8
Standard vertically focusing mirror with support points S_1 and S_2 and prop load points P_1 and P_2. L is the length of the mirror, d is the distance between the supports and t is the distance between the prop load points. F_{S1} and F_{S2} are the forces applied to the mirror at its supports, and F_{P1} and F_{P2} the forces applied by the props to compensate for the sag under gravity. The gravitational force (not shown) is applied evenly across the whole mirror.

partially compensate for the gravity-induced sag that would otherwise appear between the supports. Generally, the mirror's cross section is uniform, so that the moment of inertia $I(x) = I$ is a constant. Let the mirror have a weight W, a length L and a Young's modulus E. Because of the symmetry, the two prop load forces F_{P1} and F_{P2} are both equal to the value F_P. Then, by integrating once over each region of the mirror and imposing the conditions of (i) zero slope at the center of the mirror ($x = 0$) because of the mirror's symmetry, (ii) continuity of the slope at $x = t/2$ and $x = d/2$, one finds the slope $dy/dx =$

$$G(x) = (EI)^{-1}\left[-\tfrac{W}{6L}(x-\tfrac{L}{2})^3 - \tfrac{W}{4}(\tfrac{d}{2}-x)^2 - F_P(\tfrac{d}{2}-\tfrac{t}{2})x - \tfrac{WL^2}{48} + \tfrac{Wd^2}{16}\right] \quad \text{for } (0 < x < \tfrac{t}{2}),$$

$$G(x) = (EI)^{-1}\left[-\tfrac{W}{6L}(x-\tfrac{L}{2})^3 - \tfrac{W}{4}(\tfrac{d}{2}-x)^2 + \tfrac{F_P}{2}(\tfrac{d}{2}-x)^2 - \tfrac{WL^2}{48} + \tfrac{Wd^2}{16} - \tfrac{F_P}{8}(d^2-t^2)\right] \quad \text{for } (\tfrac{t}{2} < x < \tfrac{d}{2}), \tag{4}$$

$$G(x) = (EI)^{-1}\left[-\tfrac{W}{6L}(x-\tfrac{L}{2})^3 - \tfrac{WL^2}{48} + \tfrac{Wd^2}{16} - \tfrac{F_P}{8}(d^2-t^2)\right] \quad \text{for } (\tfrac{d}{2} < x < \tfrac{L}{2}).$$

The symmetry of the mirror makes its slope an odd function, so that slopes on the left-hand side of the mirror can be calculated by the condition $dy(x)/dx = -dy(-x)/dx$.

For mechanically bent mirrors, bending actuators are typically attached to each end of the mirror in order to vary the mirror's curvature. If a couple C_1 is applied to the end nearer the X-ray source while a different couple C_2 is applied to the end nearer the X-ray focus, the resulting slope for a mirror of uniform cross section is given by Howells & Lunt (1993) as

$$B(x) = \frac{(C_1 + C_2)x}{2EI} + \frac{(C_1 - C_2)x^2}{LEI}. \tag{5}$$

Because the differential equation that describes the bending is linear, the slope of a mirror of uniform cross section subjected to both bending couples and gravitational distortion is the sum $B(x) + G(x)$. With the addition of a uniform tilt τ, one can create a practical fitting function $S(x)$ for the measured slope of such a mirror,

$$S(x) = \tau + B(x) + G(x), \tag{6}$$

in which the four most important fitting parameters are τ, C_1, C_2 and F_P. d and t may also be included as fitting parameters, but they can be fixed or restricted to very narrow ranges as they are determined by the mirror's construction. τ is included to account for mounting errors, but it should be very close to zero. If the mirror is made from a single crystal (usually silicon) and thus has anisotropic elastic parameters, then the Young's modulus E will vary depending on the cut of the material. For silicon, E will vary between about 1.2×10^{11} and 1.8×10^{11} N m^{-2} depending on crystallographic direction (Wortman & Evans, 1965). The correct value of E must be specified when using $S(x)$ for fitting, as parameter sets with different values of E can yield fits to the same measured data with very similar χ^2 values.

A few notes should be made about the use of $S(x)$ in the analysis of experimental data on the slopes of mirrors. First, both $B(x)$ and $G(x)$ contain both linear and quadratic terms

in x. To the lowest order, these represent the curvature and ellipticity of the mirror, respectively. Therefore, it is not permissible to subtract the best-fit quadratic from the mirror's slope and attribute the remainder entirely to the gravitational distortion, because both the bending actuators and the gravitational distortion contribute to the mirror's overall curvature and ellipticity. Instead, the total function $S(x)$ must be used in order to extract the correct gravitational distortion. This is important when one wishes to reduce the gravitational distortion to a minimum. Second, although $S(x)$ is no more than cubic in x, it is not permissible to apply an ordinary cubic polynomial fit to the measured slope. This is partly because the appearance of the fitting parameters in the coefficients of more than one term imposes relationships between the coefficients that act as constraints, and also because the form of $G(x)$ depends on the region of the mirror. Finally, the appearance of quadratic terms in the fitting parameters d and t precludes the use of linear least-squares fitting techniques. Such problems require the use of non-linear least-squares techniques such as the Levenberg–Marquardt method (Levenberg, 1944; Marquardt, 1963), which in the examples below was applied through the commercial software package *OriginPro 8* (Origin, 2008).

The reader should also note that the settings of the sag compensators in the following discussion are given in units of the bending actuator length. In theory, the relationship between the actuator's length and the applied bending couple should be linear, and indeed in practice this has been sufficiently nearly linear to permit the interaction matrix method to be applied without modification. However, the calibration is often either unknown or highly uncertain and, even if it has been precisely measured in atmosphere, experience at Diamond Light Source has shown that it may be different when the mirror is in vacuum. Here again it must be emphasized that only *in situ* measurements can verify that an optical set-up works.

The fitting function $S(x)$ was first applied to pencil-beam scans taken from the collimating white-beam mirror M1 in the X-ray absorption spectroscopy optics hutch of Diamond's X-ray Spectroscopy beamline I20. This silicon mirror's length L is 1.390 m, its moment of inertia I is 1.26×10^{-6} m^4 and its weight is 133.31 N. The supports are separated by a distance d = 1.344 m, while the prop loads are separated by a distance t = 0.370–0.390 m depending slightly on the setting of the sag compensation. The ideal shape of this mirror will be a parabolic arc of slope

$$S_{\rm para}(x) = \frac{p^{1/2} - (p - x\cos\theta)^{1/2}}{(p - x\cos\theta)^{1/2}} \tan\theta, \qquad (7)$$

where p is the source–mirror distance (23.355 m) and θ is the grazing angle of incidence (2.3 mrad). The measured slope at various settings of the sag compensation mechanism, the slope's decomposition into $B(x)$ and $G(x)$, and the residual are shown in Fig. 9 for fits to $S(x)$ taken with $E = 1.8 \times 10^{11}$ N m^{-2}. The values of $|\tau|$ derived from the fits were all very small ($\leq$3.14 µrad) and so are not shown. Two results are especially noteworthy. First, the decomposition in Fig. 9 shows the sag compensation setting at which the gravitational distortion is least, namely −1.5 mm. Second, the residuals of the fits, which show the degree to which this simple theory of elastic bending fails to account for the mirror's shape, are both small (±1 µrad) and largely independent of the sag compensator's setting. Among the factors excluded from the model are polishing and clamping errors. While such errors can be partially corrected by using the bending actuators and the sag compensator, the residuals of the fits provide an estimate of the polishing and clamping errors that *cannot* be compensated. Note once more the consistency of the residuals over a wide range of sag compensation settings, even for these *in situ* measurements of this complex mechanism.

A second type of analysis that can be done on the measured slopes is the calculation of the best-fit quadratic to the absolute slope error, which is the measured slope minus the ideal slope $S_{\rm para}$. It is important to recognize that this does not yield the gravitational distortion for the reasons discussed above. However, since $B(x)$ for a rectangular beam of uniform cross section is purely quadratic in x, the coefficients of the best-fit quadratic will yield the changes δC_1 and δC_2 that should be made to the bending couples to minimize the remaining slope error. The residual absolute slope error remaining after subtraction of the best-fit quadratic is shown in Fig. 10 along with the required changes to the bending couples. The absolute slope error and its residual are both strongly dependent on the sag compensation setting. The mirror's absolute slope error is shown to be best corrected by the bending actuators when the sag compensation is set to −2.5 mm. It should be stressed that the bending actuators alone are thus proven to be insufficient to remove the distortion caused by gravitational sag; instead, it is critically important to find the correct setting of the sag compensation. Once this was done, the residual figure error at this optimal setting could be calculated by numerical integration of the residual absolute slope error. Fig. 10 also shows this result. Although the agreement with factory data provided by the mirror's manufacturer before shipment to Diamond is not close, the figure errors are still of the same order of magnitude, indicating that reasonable estimates of polishing and clamping errors have indeed been extracted from the *in situ* measurements.

Later *in situ* optimization of this mirror using the interaction matrix method (Hignette *et al.*, 1997) on pencil-beam scans taken one year after those displayed in this section yielded an optimal sag compensation setting of −2.171 mm, fully consistent with the above analysis despite the long interval. However, the first application of the interaction matrix method to a mechanical mirror at Diamond Light Source was made for the I15 VFM. For this reason, and also because the improvement achieved thereby at I15 was so dramatic, this case will be the topic of the next section.

3.2.2. Improvement in performance of the I15 VFM. The design shown in Fig. 8 also applies to the VFM in the Extreme Conditions beamline I15. This mirror had been achieving a good focus only when its central section was illuminated, while the edges of the mirror were producing strong beamlets both

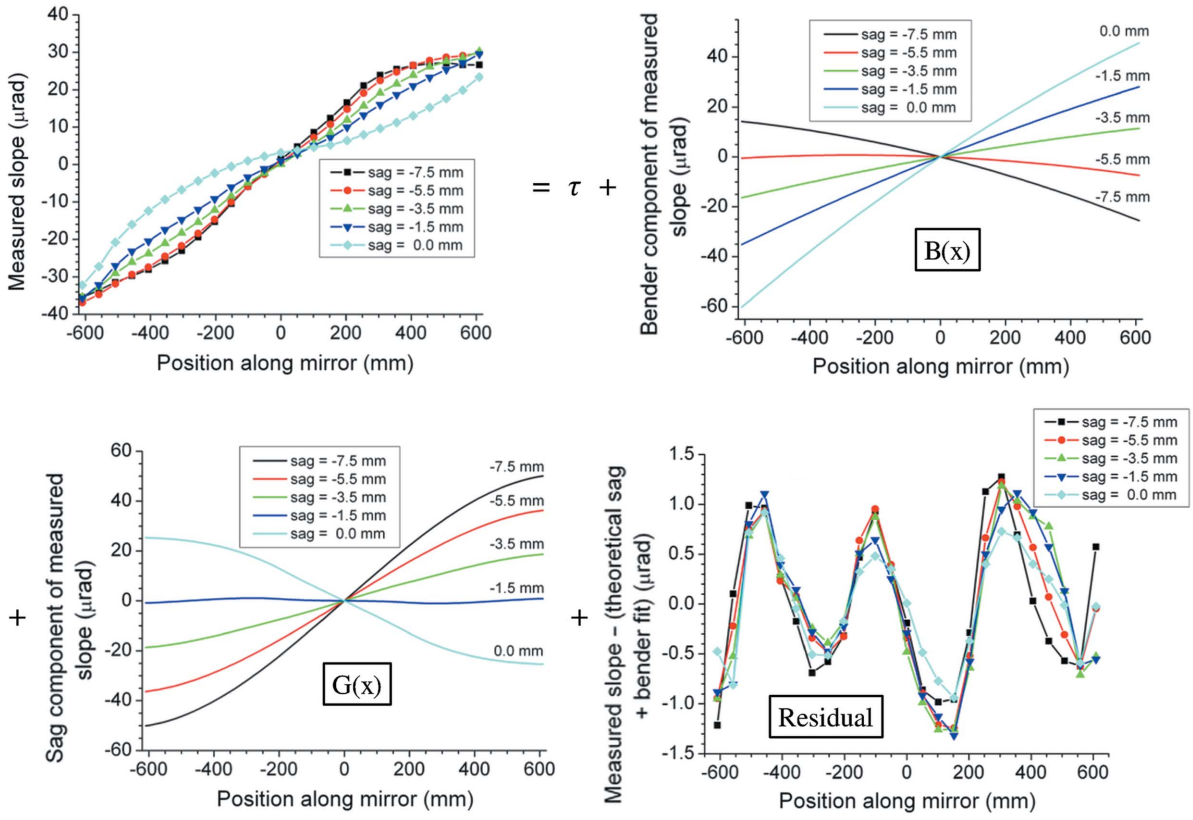

Figure 9
Decomposition of the slope of the I20 collimating mirror M1 measured by the pencil-beam method (upper left) into the bender component $B(x)$ (upper right), the sag component $G(x)$ (lower left) and the residual (lower right). Fixed and bounded parameter values are given in the text.

above and below the main spot (Fig. 11). Pencil-beam scans were used to determine both the initial slope error of the I15 VFM and its response to changes in the setting of the upstream actuator, the downstream actuator and the gravitational sag compensator. It must be noted that the responses do not depend exactly linearly on the change in each motor's setting as is theoretically required for the usual calculation of the motor corrections, which uses multiple linear regression. Nevertheless, by using the average responses, it was possible to obtain much enlightening information. Fig. 12 shows the following: (i) a pencil-beam measurement of the I15 VFM's initial state; (ii) a calculation using the motor corrections derived from the usual optimization procedure; (iii) a calculation of the motor corrections that yielded the least simulated slope error in the central region, used because the sag compensator lacked sufficient range to be adjusted as far

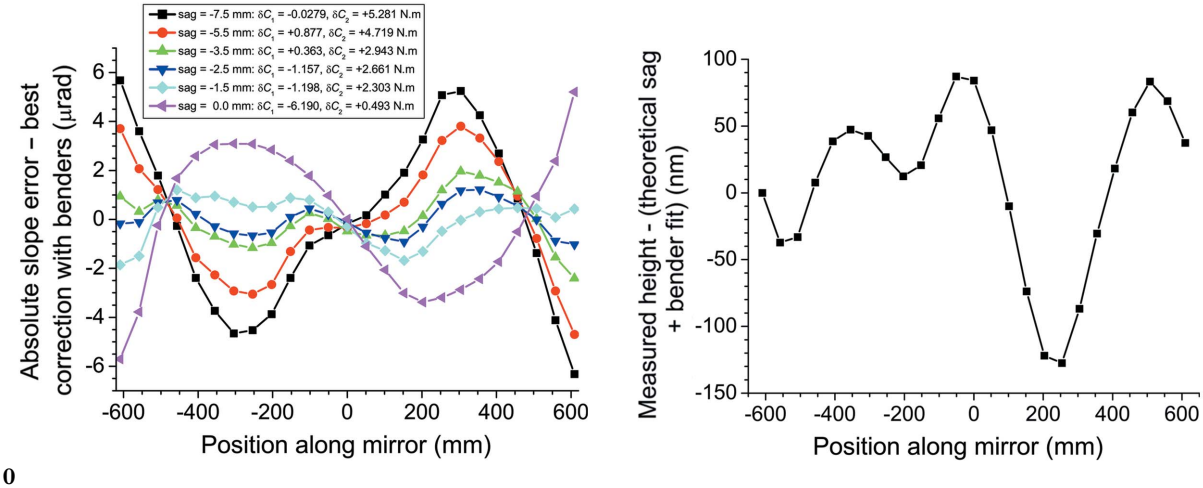

Figure 10
(*a*) Remaining slope error of the I20 mirror M1 after best correction with bending actuators alone. See text for details. (*b*) Figure error calculated by integrating the residual of the slope error measured *in situ* on the I20 mirror M1 for a sag compensation setting of −2.5. This did not exactly match the manufacturer's data but is of the same order of magnitude.

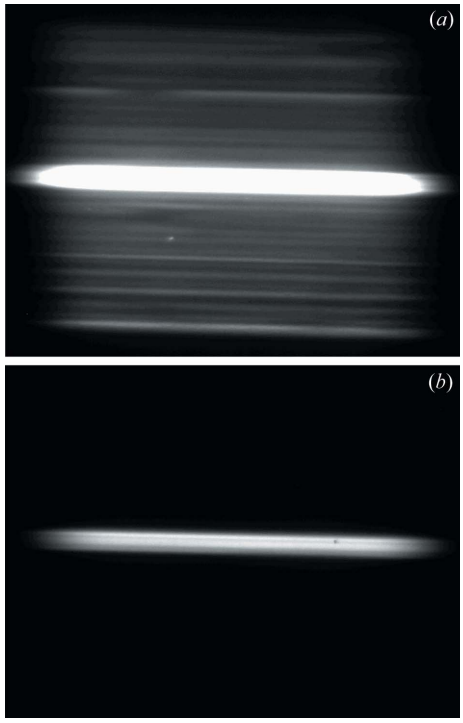

Figure 11
Focused beam profile of I15 VFM with (*a*) illumination of whole mirror and (*b*) illumination limited to central section, as taken by the in-house X-ray camera (Sutter *et al.*, 2011). Both images are on the same scale, with the total height of each image equal to 1853 µm. Because the gravitational sag of this mirror was maladjusted at the time, a good focus could be obtained only by limiting the illuminated length of the mirror (see text).

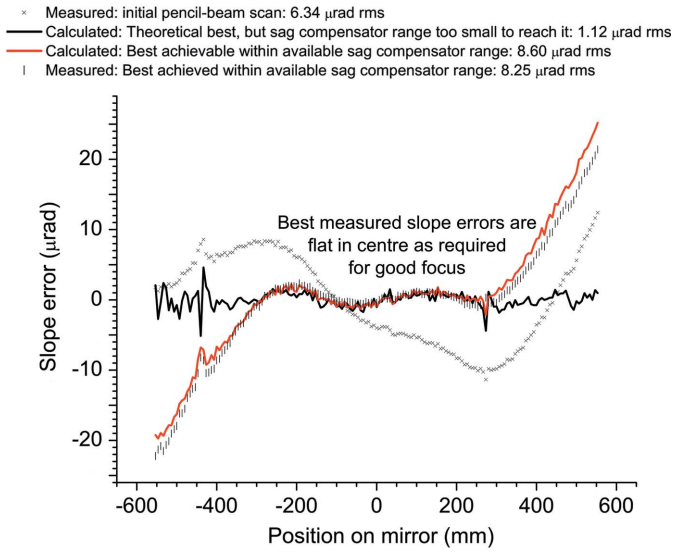

Figure 12
Pencil-beam scan data of the initial state of the I15 VFM, a calculation of the best achievable slope error using the optimization procedure with the average responses of the motors, a calculation of the best achievable slope error in the central region using then attainable values of the sag compensation, and pencil-beam scan data of the final state of the I15 VFM.

as the optimization procedure indicated; (iv) a pencil-beam measurement using approximately the motor corrections in the previous calculation.

As indicated by the beam images, only the central region of the mirror has the correct curvature, while both ends have a markedly incorrect curvature. As long as the sag correction δ(GS) was kept at +1.9 mm, simulations showed no way to remedy the curvature at the edges by using the bending actuators alone. According to the optimization procedure, the only way to reduce the mirror's slope errors was to apply a sag correction δ(GS) of +45.87 mm, far beyond the range of the sag compensation mechanism at the time of these measurements. Acting on this knowledge, the I15 beamline team replaced the preloading springs in the sag compensation mechanism with softer ones and added a stiffer spring to the sag compensation motor to increase its range. This course of action proved successful. Fig. 13 shows the final results of a second series of measurements made after applying the optimization procedure: a set of pencil-beam scans, an image of the vertically focused beam taken with the in-house X-ray camera (Sutter *et al.*, 2011), and a vertical scan taken with a 20 µm pinhole. This time the mirror could accept the entire beam and focus it into a high-quality spot, without the top and bottom beamlets visible before the springs were adjusted. Furthermore, the remaining r.m.s. slope error (0.728 µrad) is now well below the 1 µrad level that was acceptable for most Diamond Light Source beamlines. On the other hand, because the focal spot is quite far from the VFM (17.295 m), the remaining slope error leaves clearly explainable structure in the focal profile measured by the pinhole scan: (i) left-hand shoulder: troughs in the pencil-beam scan; (ii) middle peak: middle and far right peaks in the pencil-beam scan; (iii) right-hand shoulder: leftmost peak in the pencil-beam scan.

4. Conclusions

The results of this paper show that much valuable information about focusing and collimating active mirrors can be obtained from the *in situ* pencil-beam method without any need to remove them from their operating environment and without any complex apparatus. For frequent inspections under operating conditions, or when the mirrors are contained in a large mechanical frame, *in situ* methods are the only option. The pencil-beam method has successfully served diverse aims: as an acceptance test of a newly polished mirror, as a quick and accurate check of the mirror figure that can be performed at the beamline scientist's convenience, and as a test of a mechanically bent mirror's bending actuators and sag compensator. New methods of analysis have also improved understanding of the performance of mechanically bent mirror systems. Structures within the focal spot of the I15 VFM could be traced to specific regions of the mirror, while the slope of the I20 vertically collimating mirror could be fit to theoretical treatments of bending under gravity and applied couples, allowing the best setting of the sag compensator to be determined. These experiences with both I15 and I20 indicate that the bending actuators of a mechanically bent mirror cannot alone compensate for the distortion caused by gravity.

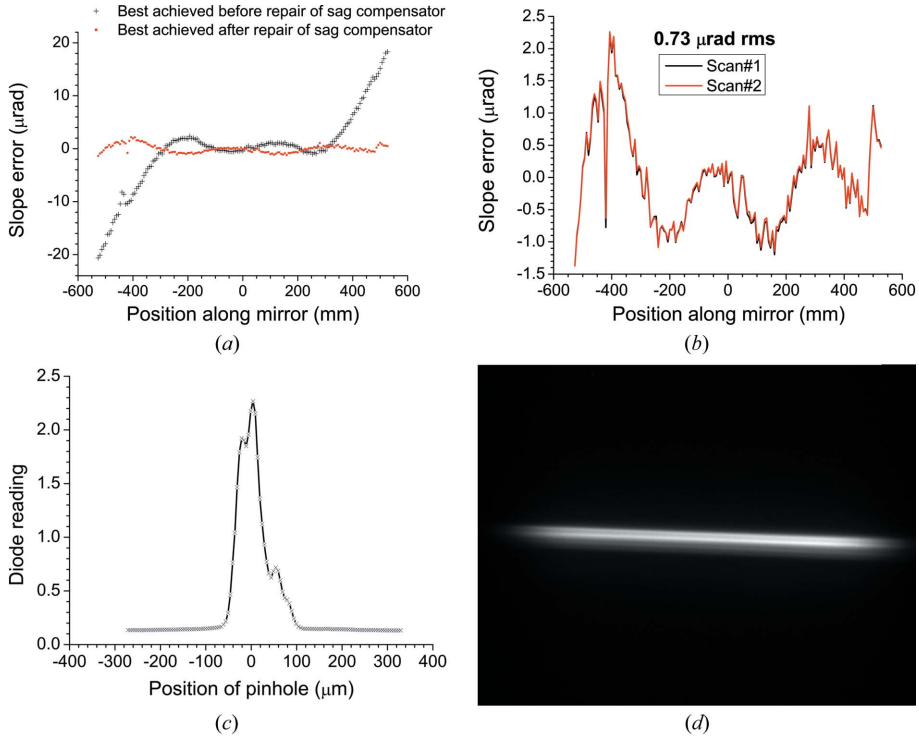

Figure 13
For the I15 VFM, (*a*) best measured slope error before and after repair of the sag compensator. (*b*) Two consecutive pencil-beam scans after the repair, showing both excellent reproducibility and low remaining slope errors after application of the optimization procedure. (*c*) Scan of vertical focal profile with 20 μm pinhole taken after repair of the sag compensator and optimization of the motors. (*d*) Image taken by the in-house X-ray camera of the focused beam that was measured with the pinhole scan. This image has the same size and scale as those in Fig. 11. Note that in both the pinhole scan and the image the whole length of the mirror was illuminated.

Instead, first the setting of the sag compensator that least distorts the mirror should be found. Only then should the bending actuators be used to set the mirror's shape.

The authors thank all the Diamond Light Source beamline teams from whose mirrors these results were collected. They are Thomas Sorensen, Juan Sanchez-Weatherby and James Sandy of I02; Katherine McAuley, James Nicholson and Mark Williams of I03; David Hall and Ralf Flaig of I04; Dave Allan, Harriott Nowell, Kirsten Christensen, Sarah Barnett and Anna Warren of I19; Nick Terrill, Marc Malfois, Katsuaki Inoue and Jen Hiller of I22; Heribert Wilhelm, Andrew Jephcoat and Annette Kleppe of I15; and Sofía Díaz-Moreno, Shusaku Hayama, Mónica Amboage and Adam Freeman of I20.

References

Alcock, S. G., Sawhney, K. J. S., Scott, S., Pedersen, U., Walton, R., Siewert, F., Zeschke, T., Senf, F., Noll, T. & Lammert, H. (2010). *Nucl. Instrum. Methods Phys. Res. A*, **616**, 224–228.
EPICS (2010). *Experimental physics and industrial control system*, http://www.aps.anl.gov/epics.
Hignette, O., Freund, A. & Chinchio, E. (1997). *Proc. SPIE*, **3152**, 188–199.
Howells, M. R. & Lunt, D. (1993). *Opt. Eng.* **32**, 1981–1989.
Koch, A., Raven, C., Spanne, P. & Snigirev, A. (1998). *J. Opt. Soc. Am. A*, **15**, 1940–1951.
Levenberg, K. (1944). *Q. Appl. Math.* **2**, 164–168.
Marquardt, D. W. (1963). *J. Soc. Indust. Appl. Math.* **11**, 431–441.
Martin, T. & Koch, A. (2006). *J. Synchrotron Rad.* **13**, 180–194.
OpenGDA (2010). *GDA – Software for Science*, http://www.opengda.org/OpenGDA.html.
Origin, (2008). *OriginPro 8 SR4 v8.0951*. OriginLab Corporation, One Roundhouse Plaza, Northampton, MA 01060, USA (http://www.OriginLab.com). (Copyright 1991–2008.)
Qian, S., Jark, W., Takacs, P. Z., Randall, K. J. & Yun, W. (1995). *Opt. Eng.* **34**, 396–402.
Roark, R. J. & Young, W. C. (1975). *Formulas for Stress and Strain*, 5th ed., ch. 7. New York: McGraw-Hill.
Sutter, J. P., Alcock, S. G. & Sawhney, K. J. S. (2011). *Proc. SPIE*, **8139**, 813906.
Timoshenko, S. P. (1921). *Philos. Mag. Ser. 6*, **41**, 744–746.
Timoshenko, S. P. (1922). *Philos. Mag. Ser. 6*, **43**, 125–131.
Wortman, J. J. & Evans, R. A. (1965). *J. Appl. Phys.* **36**, 153–156.